

Exceptional Degeneracies in Traveling Wave Tubes with Dispersive Slow-Wave Structure Including Space-Charge Effect

Kasra Rouhi¹, Robert Marosi¹, Tarek Mealy¹, Ahmed F. Abdelshafy¹, Alexander Figotin², and Filippo Capolino¹

¹Department of Electrical Engineering and Computer Science, University of California, Irvine, CA 92697 USA

²Department of Mathematics, University of California, Irvine, CA 92697 USA

The interaction between a linear electron beam and a guided electromagnetic wave is studied in the context of exceptional points of degeneracy (EPD) supported by such an interactive system. The study focuses on the case of a linear beam traveling wave tube (TWT) with a realistic helix waveguide slow-wave structure (SWS). The interaction is formulated by an analytical model that is a generalization of the Pierce model, assuming a one-dimensional electron flow along a dispersive single-mode guiding SWS and taking into account space-charge effects in the system. The augmented model using phase velocity and characteristic impedance obtained via full-wave simulations is validated by calculating gain versus frequency and comparing it with that from more complex electron beam simulators. This comparison also shows the accuracy of our new model compared with respect to the non-dispersive Pierce model. EPDs are then investigated using the augmented model, observing the coalescence of complex-valued wavenumbers and the system's eigenvectors. The point in the complex dispersion diagram at which the TWT-system starts/ceases to exhibit a convection instability, i.e., a mode starts/ceases to grow exponentially along the TWT, is the EPD. We also demonstrate the EPD existence by showing that the Puiseux fractional power series expansion well approximates the bifurcation of the dispersion diagram at the EPD. This latter concept also explains the "exceptional" sensitivity of the TWT-system to changes in the beam's electron velocity when operating near an EPD.

HIGH power traveling wave tube (TWT) amplifiers are of high importance for telecommunications, high-performance radar applications, including atmospheric studies, precision tracking, and high-resolution imaging [1], [2], [3]. A TWT uses a slow-wave structure (SWS) as a key component to harvest energy from an electron beam (e-beam) into radio frequency waves efficiently over broad bandwidths [4], [5]. In this paper, we focus on a realistic helix TWT with dispersive SWS's characteristic parameters. The interaction with the e-beam affects the way EM waves propagate in the so-called "hot" circuit, i.e., accounting for the beam-electromagnetic (EM) mode interaction.

An exceptional point of degeneracy (EPD) in a system refers to the property of the relevant system matrix that contains at least one nontrivial Jordan block structure, i.e., when two or more eigenvectors coalesce into a single degenerate one [6], [7], [8], [9], [10]. The concept of EPD has been studied in lossless, spatially [11], [12], or temporally [13], [14] periodic structures, and in systems with loss and/or gain under parity-time symmetry [15], [7], [16]. We employ the Puiseux fractional power expansion series to illustrate the bifurcation of the system's dispersion diagram at the EPD [17]. The EPD has been studied for its applications in sensing devices [18], [19] and oscillators [20], [21], [22], [23].

In [24], the EPD in a system of an e-beam interacting with an EM mode guided in a non-dispersive SWS with distributed power extraction and without accounting for electrons' debunching is used to conceive an effective oscillator. The mathematical formulation in [25] does not include waveguide dispersion in the model, and above all, it cannot capture the second EPD that occurs in the real TWTs at a higher frequency (See Fig. 4). This paper explains the fundamental physics describing the TWT operation, accounting for electrons' debunching caused by space-charge effects and SWS frequency dispersion, and describes the bifurcation points in the dispersion diagram

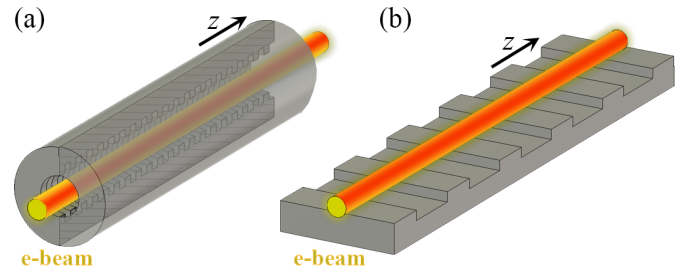


Fig. 1. Illustrative schematics showing an e-beam in the proximity of an EM-guiding SWS. (a) Beam inside a circular waveguide with corrugations, and (b) beam near a periodic grating.

using the coalescence of the system's eigenvectors. Also, the EPD-related fractional power expansion is used to explain the wavenumber's extreme sensitivity to perturbations to the system parameters such as operating frequency and e-beam's velocity and how EPDs are related to the TWT amplification bandwidth. We calculate the characteristic parameters of the cold guiding SWS based on what Pierce proposed in [26], [27], [28] and further developed for frequency-dependent TWT-systems in analogy (but differently) to what done in [29], [30].

The system consists of an EM field in a guiding SWS interacting with a single e-beam flowing in the z -direction is schematically shown in Fig. 1. The e-beam's electrons have average velocity and linear charge density u_0 and ρ_0 , respectively. The e-beam has an average current $I_0 = -\rho_0 u_0$ and an equivalent kinetic non-relativistic d.c. voltage $V_0 = u_0^2/2\eta$, where $\eta = e/m = 1.758820 \times 10^{11}$ C/Kg is the charge-to-mass ratio of the electron with charge $-e$ and rest mass m . The small-signal modulation in the e-beam velocity and charge density u_b and ρ_b , respectively, describe the so-called "space-charge wave". The a.c. beam current and equivalent voltage are given by $i_b = u_b \rho_0 + u_0 \rho_b$ and $v_b = u_b u_0 / \eta$, where

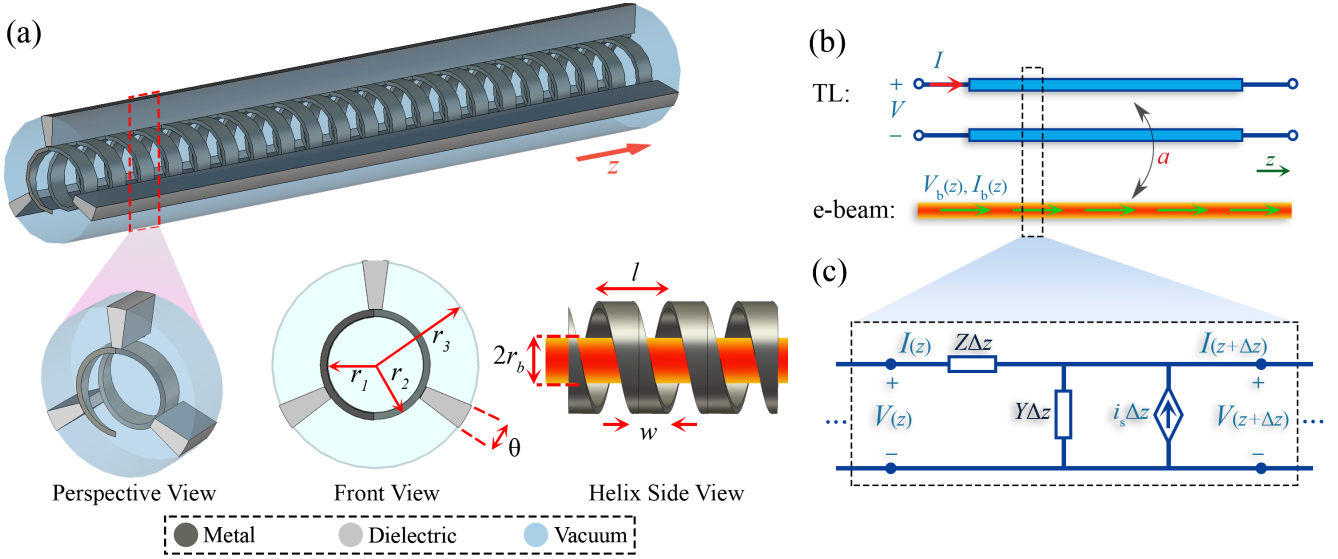


Fig. 2. (a) Tape helix SWS in a circular metallic waveguide with radius $r_3 = 1.06$ mm. An e-beam with radius $r_b = 560$ μm flows along the axis of the helical conductor of inner radius $r_1 = 744$ μm , and outer radius $r_2 = 846$ μm supported by dielectric rods. The other geometric parameters are $l = 1.04$ mm, $w = 520$ μm , and $\theta = 14.2^\circ$. (b) Schematic of the equivalent TL coupled to the e-beam used to study the hybrid EM-space charge wave. (c) Equivalent TL circuit showing the per-unit-length impedance, admittance and current generator i_s that represents the effect of the e-beam on the TL.

we have retained only the linear terms based on the small-signal approximation [27], as also explained in Appendix A. We implicitly assume a time dependence of $\exp(j\omega t)$, so the a.c. space-charge wave modulating the e-beam is described in the phasor domain with $V_b(z)$ and $I_b(z)$, as

$$\partial_z V_b = -j\beta_0 V_b - aZI - j\frac{I_b}{A\epsilon_0\omega}, \quad (1)$$

$$\partial_z I_b = -jgV_b - j\beta_0 I_b, \quad (2)$$

where $\beta_0 = \omega/u_0$ is the phase constant of the space-charge wave (when neglecting plasma frequency effects), $g = I_0\beta_0/(2V_0)$, Z is the equivalent TL distributed series impedance, and $I(z)$ is the equivalent TL current, as will be explained later. Furthermore, $E_z = E_w + E_p = aZI + jI_b/(A\epsilon_0\omega)$ is the longitudinal polarization (in the z -direction) of the electric field component that modulates the velocity and bunching of the electrons. The longitudinal field $E_z = E_w + E_p$ is the sum of two components. The term E_p accounts for nonuniform charge density, and in the phasor form is given by $E_p = jI_b/(A\epsilon_0\omega)$ [31, Chapter 10], where A is the e-beam cross-sectional area, and ϵ_0 is vacuum permittivity. The term E_p is generated by charge distribution that also causes the so-called “debunching”, and its calculation is in agreement with the Lagrangian model for TWT-systems in [32, Chapter 7], as explained in Appendix G. In addition, the term $E_w = aZI$ is the longitudinal electric field of the EM mode propagation in the SWS, affecting the bunching of the e-beam, according to the well-known Pierce model [27]. Also, the term a represents a coupling strength coefficient, that describes how the e-beam couples to the TL as already introduced in [33] and [34], [32, Chapter 3]. More details on the fundamental equations describing the interacting system are in Appendix B. The well-known telegrapher’s equations

describe the EM modal propagation in the SWS, based on the equivalent TL model shown in Figs. 2(b) and (c) where the distributed per-unit-length series impedance Z , and shunt admittance Y relate the equivalent TL voltage $V(z)$ and current $I(z)$ phasors as

$$\partial_z V = -ZI, \quad (3)$$

$$\partial_z I = -YV - a\partial_z I_b. \quad (4)$$

Here, the term $i_s = -a\partial_z I_b$ represents a distributed current generator [35], that accounts for the effect of the beam’s charge wave flowing in the SWS [27], [33]. In order to construct an accurate model that provides precise predictions for realistic structures and overcome the simplicity of the ideal assumptions in the original Pierce model, we use frequency-dependent waveguide parameters in the equations. In practice, we first analyze wave propagation in the “cold” SWS (i.e., in the absence of the e-beam) using a full-wave method to get the values of $Z(\omega)$ and $Y(\omega)$ to be used in the formulation. To recover these frequency-dependent characteristic parameters, we use the finite element method eigenmode solver in CST Studio Suite and extract the cold circuit EM phase velocity $v_c(\omega) = \omega/\beta_c(\omega)$, where $\beta_c(\omega) = \sqrt{-Z(\omega)Y(\omega)}$ is the phase propagation constant of the cold SWS mode, and the equivalent TL characteristic impedance $Z_c(\omega)$. By using the extracted values for $v_c(\omega)$ and $Z_c(\omega)$, the equivalent frequency-dependent distributed series impedance $Z(\omega) = j\omega Z_c(\omega)/v_c(\omega) = jZ_c(\omega)\beta_c(\omega)$ and shunt admittance $Y(\omega) = j\omega/(Z_c(\omega)v_c(\omega)) = j\beta_c(\omega)/Z_c(\omega)$ are calculated. Moreover, in Eq. (4), when $a = 0$ the e-beam is not coupled to the TL, and when $a = 1$, the model reduces to the one developed in [27], [28]. The presence of this coupling strength coefficient generalizes what was done in [27], [28],

since the beam may be subject to a strong longitudinal electric field that is not accurately accounted for by the simple circuit impedance Z_c of the originally Pierce model [27], [28]. For convenience, we define a state vector $\Psi(z) = [V, I, V_b, I_b]^T$ that describes the hybrid EM-space charge wave propagation along z , and rewrite Eqs. (1), (2), (3), and (4) in matrix form as

$$\partial_z \Psi(z) = -j \underline{\mathbf{M}} \Psi(z), \quad (5)$$

where $\underline{\mathbf{M}}$ is the 4×4 system matrix that after replacing $v_c(\omega)$ and $\beta_c(\omega)$ in the system equations, reads as

$$\underline{\mathbf{M}} = \begin{bmatrix} 0 & \beta_c(\omega) Z_c(\omega) & 0 & 0 \\ \beta_c(\omega)/(Z_c(\omega)) & 0 & -ag & -a\beta_0 \\ 0 & a\beta_c(\omega) Z_c(\omega) & \beta_0 & R_p \\ 0 & 0 & g & \beta_0 \end{bmatrix}. \quad (6)$$

In the above system matrix, R_p is a space-charge parameter related to the debunching of beam's charges, and is given by [36], [37]

$$R_p = \frac{1}{A\varepsilon_0\omega} = \frac{2V_0\omega_q^2}{\omega I_0 u_0}, \quad (7)$$

where $\omega_q = R_{sc}\omega_p$ is the reduced plasma angular frequency, $\omega_p = \sqrt{-\rho_0\eta/(A\varepsilon_0)} = \sqrt{I_0 u_0/(2V_0 A\varepsilon_0)}$ is the plasma frequency [38], and R_{sc} is the plasma frequency reduction factor [39]. The term R_{sc} accounts for reductions in the magnitude of the axial component of the space-charge electric field due to either finite beam radius or proximity of the surrounding conducting walls. Fields produced by space-charges represent repulsive forces in a dense beam of charged particles. Assuming a state vector z -dependence of the form $\Psi(z) \propto \exp(-jkz)$, where k is the wavenumber of a hybrid mode in the EM-space charge wave interacting system, the eigenmodes are obtained by solving the eigenvalue problem $k\Psi(z) = \underline{\mathbf{M}}\Psi(z)$. The resulting modal dispersion characteristic equation is given by

$$\begin{aligned} D(\omega, k) &= \det(\underline{\mathbf{M}} - k\underline{\mathbf{I}}) = k^4 - k^3(2\beta_0) \\ &+ k^2(\beta_0^2 - \beta_q^2 - \beta_c^2(\omega) + a^2g\beta_c(\omega)Z_c(\omega)) + k(2\beta_c^2(\omega)\beta_0) \\ &- \beta_c^2(\omega)(\beta_0^2 - \beta_q^2) = 0. \end{aligned} \quad (8)$$

where $\beta_q = \omega_q/u_0 = \sqrt{R_p g}$ is the phase constant of space-charge wave traveling with a phase velocity equal to u_0 and at an angular frequency equal to ω_q . The solution of Eq. (8) leads to four modal complex-valued wavenumbers that describe the modes in the TWT interactive system. The above characteristic equation is equivalently rewritten as

$$(k^2 - \beta_c^2)((k - \beta_0)^2 - \beta_q^2) = -a^2g\beta_c(\omega)Z_c(\omega)k^2. \quad (9)$$

The first parenthesis on the left side of Eq. (9) only contains parameters related to TL and the second parenthesis includes only the parameters of the e-beam. The term on the right side represents the interaction between the EM mode in the

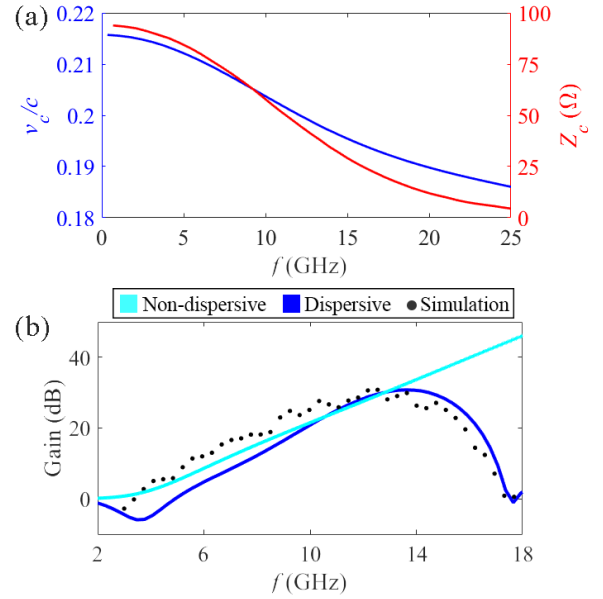


Fig. 3. (a) Phase velocity and Pierce impedance of the EM mode in the cold SWS, obtained via full-wave eigenmode simulations. (b) Gain versus frequency from the theoretical model based on the non-dispersive (cyan curve), and dispersive (blue curve) solution of system in Eq. (5), and simulation results using the software LATTE (black dots).

SWS and the e-beam, and it contains both e-beam and EM mode parameters. When the e-beam and TL are decoupled, one has $a = 0$, the two equations in parenthesis become two independent dispersion equations.

A second-order EPD occurs when two eigenmodes coalesce in their eigenvalues and eigenvectors. Thus, when such degeneracy occurs, the matrix $\underline{\mathbf{M}}$ is similar to a matrix that contains a Jordan block of order two. A necessary condition to have a second-order EPD is to have two repeated eigenvalues, which means that the characteristic equation should have two repeated roots as

$$D(\omega_e, k) \propto (k - k_e)^2, \quad (10)$$

where ω_e and k_e are the degenerate angular frequency and wavenumber at the EPD. This happens when $D(\omega_e, k_e) = 0$, and $\partial_k D(\omega_e, k)|_{k=k_e} = 0$. We derive the following expressions for $Z = Z_e$ and $Y = Y_e$, which will produce the EPD for given e-beam parameters

$$Z_e = \frac{j((k_e - \beta_0)^2 - R_p g)^2}{a^2 g(-\beta_0^2 + k_e \beta_0 + R_p g)}, \quad (11)$$

$$Y_e = \frac{j a^2 g k_e^3 (k_e - \beta_0)}{((k_e - \beta_0)^2 - R_p g)^2}, \quad (12)$$

where all the parameters are calculated at ω_e and k_e . Assuming that the EPD conditions for impedance and admittance in Eqs. (11) and (12) are satisfied, the degenerate wavenumber k_e is determined by the product of Eqs. (11) and (12)

$$Z_e Y_e = \frac{-k_e^3 (k_e - \beta_0)}{(-\beta_0^2 + k_e \beta_0 + R_p g)}. \quad (13)$$

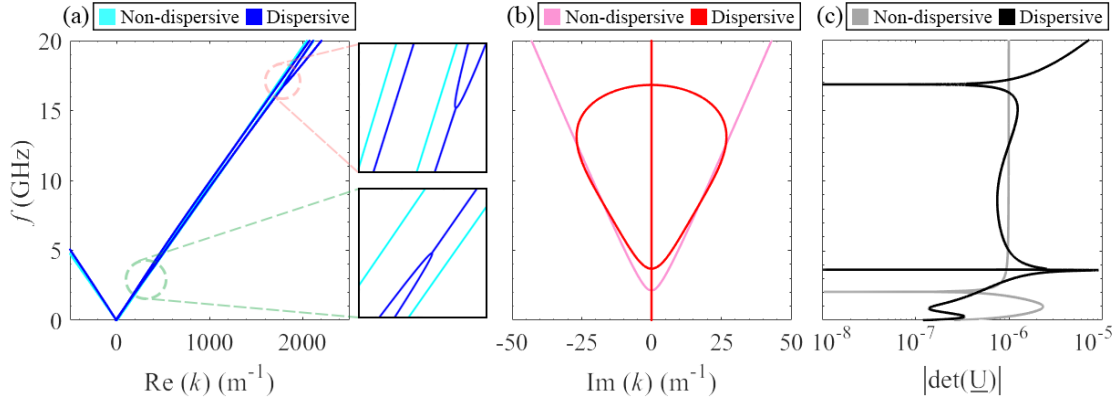


Fig. 4. Dispersion diagram of the four complex-valued wavenumbers versus frequency, which shows two (one) bifurcation points correspond to the EPDs in the dispersive (non-dispersive) system, and $|\det(\underline{U})|$ whose minima indicate the occurrence of EPDs.

We know that $\beta_{c,e}^2 = -Z_e Y_e$ and $\beta_q^2 = R_p g$ under the EPD condition, so we will calculate the wavenumber of the degenerate hybrid mode k_e by solving

$$\beta_{c,e}^2 \beta_q^2 = (k_e^3 - \beta_{c,e}^2 \beta_0)(k_e - \beta_0). \quad (14)$$

In order to investigate the EPD, we analytically derive the system's eigenvector expressions related to the four wavenumbers k_n with $n = 1, 2, 3, 4$, that are written in the form of

$$\Psi_n = \begin{bmatrix} (k_n - \beta_0)^2 - \beta_q^2 \\ \frac{k_n}{\beta_c Z_c} ((k_n - \beta_0)^2 - \beta_q^2) \\ a k_n (k_n - \beta_0) \\ a g k_n \end{bmatrix}. \quad (15)$$

In summary, the two conditions in Eqs. (11) and (12) represent constraints on the TL parameters, calculated at the EPD frequency. These two conditions need to be enforced to have a second-order EPD, where two eigenmodes of the interacting system have identical eigenvalues $k_1 = k_2 = k_e$ and eigenvectors $\Psi_1 = \Psi_2 = \Psi_e$. Suppose we find a set of parameters to satisfy the EPD condition; in that case, these values lead to the same two eigenvalues and a single corresponding eigenvector according to Eq. (15).

The helix SWS features a conventional two-body (input and output) cylindrical vacuum envelope that contains a metallic tape helix supported by three equally spaced dielectric rods, which are made of BeO with $\epsilon_r = 6.5$ [40]. The SWS is illustrated in Fig. 2(a), with the helix's geometric parameters shown in the caption. Because the helix TWT dispersion is vital for pulse amplification or nonstationary problems' response of the tube, the frequency dependence of the cold circuit phase velocity and the interaction impedance must be included in the model [29], [30], [41]. We have simulated the helix SWS by using the finite element method eigenmode solver in CST Studio Suite and extracted the characteristic parameters, i.e., the cold circuit EM phase velocity $v_c(\omega)$, and the equivalent TL characteristic impedance $Z_c(\omega)$; then the calculated results is illustrated in Fig. 3(a). We demonstrate the occurrence of EPDs in the helix TWT using practical values for both the helix SWS and e-beam. For the e-beam, we assume $u_0 = 0.2c$, where c is the speed of light, $I_0 = 47$ mA,

$V_0 = 10.5$ kV, and a e-beam radius equal to $r_b = 560$ μm . The resulting plasma frequency is $f_p = \omega_p / (2\pi) = 624.6$ MHz. We assume a plasma frequency reduction factor of $R_{sc} = 0.12$, which was calculated for the SWS in Fig. 2(a) using the software LATTE [42], [29], [43]. The maximum interaction between the space-charge wave and the EM wave occurs when they are synchronized, i.e., by matching v_c to u_0 , a condition that is specifically called ‘‘synchronization’’. We calibrate the value of the coupling strength coefficient a , which is an essential parameter of our model, to predict the gain in the TWT; this coefficient can be used to calculate the gain of longer TWT structures. In this example, we estimate $a = 0.527$, as extracted from simulations, and the required steps are explained in Appendix E. Then, by solving the wavenumber dispersion equation for specific frequency values, we obtain the real and imaginary parts of the four hybrid wavenumbers in Fig. 4(a) and (b). Moreover, in Fig. 4, we illustrate the non-dispersive results by using an average value of v_c and Z_c in the predetermined frequency range (See Fig. 3(a)). As we can observe, the non-dispersive model cannot capture the second EPD at a higher frequency, which exists in realistic structures.

The similarity transformation matrix $\underline{U} = [\underline{U}_1, \underline{U}_2, \underline{U}_3, \underline{U}_4]$, where the column \underline{U}_i is the eigenvector corresponding to the i -th eigenvalue, diagonalizes the system matrix as $\underline{M} = \underline{U} \underline{\Lambda} \underline{U}^{-1}$. At an EPD, at least two eigenvectors become linearly dependent, implying that $|\det(\underline{U})|$ vanishes. In this example, we consider the EPD frequency of the dispersive model at $f_e = 16.82$ GHz in the shown frequency range, where $\beta_{0,e} = 1762.21$ m^{-1} . In Fig. 4(a) and (b), we observe the bifurcation of the wavenumbers' real and imaginary parts at the EPDs. The maximum TWT gain is at $f_{opt} = 13.14$ GHz, where the maximum value of the imaginary part occurs. This frequency is close to the initial-design synchronization frequency $f_{sync} = 12.10$ GHz, where $v_c = u_0 = 0.2c$, as expected. It may be possible to shift the maximum gain frequency by changing the frequencies of EPDs through varying plasma frequency or other controllable parameters in the TWT-system. In order to validate the proposed TWT model, which accounts for waveguide mode dispersion and space-charge effect, we provide the gain

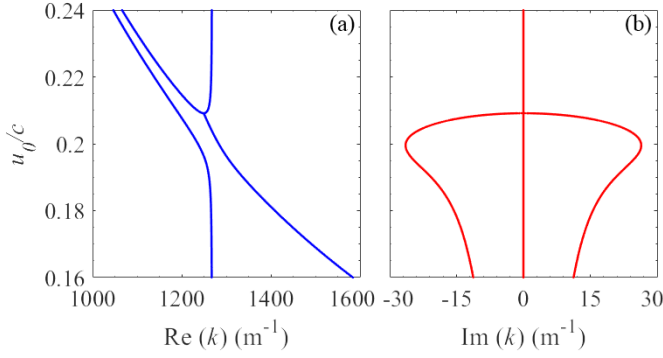


Fig. 5. Dispersion diagram of the three wavenumbers versus u_0 . The diagram shows a bifurcation point that corresponds to the EPD point, whereas frequency is equal to the synchronization frequency f_{sync} .

versus frequency plot obtained from simulations in LATTE and compare it to the theoretically calculated gain based on applying boundary conditions for the charge wave and EM mode as explained in Appendix E. We observe a good agreement between simulated and theoretical results for the dispersive model in Fig. 3(b), which demonstrates the accuracy of the proposed method. This figure shows that the non-dispersive model cannot predict the gain correctly in the illustrated frequency range.

So far, we have analyzed the dispersion diagram by varying frequency. In the next step, we investigate the wavenumber dispersion diagram varying the electron's average velocity out of synchronization and observe EPDs under these conditions. Hence, we assume the frequency to be fixed and equal to the original synchronization frequency f_{sync} . Then, we change u_0 to explore EPDs out of synchronization, leading to the results in Fig. 5. In this figure, only wavenumbers with a positive real part are displayed as mentioned in [44], and a second-order EPD exists around $u_{0,e} = 0.209c$. So the bifurcation is observed in the dispersion diagram when we select u_0 larger than v_c . The bifurcation of the wavenumber, when u_0 is varied, is clear evidence of an EPD.

Based on the results in Figs. 4 and 5, we conclude that the TWT-system is very sensitive to variation in frequency and u_0 near an EPD. Fig. 6 shows the $\log(|\det(\underline{\mathbf{U}})|)$ when frequency and u_0 are varied. The black curve shows the lowest values, which means the eigenvectors coalesce at those specific values of f and u_0 . Thus, the black contour represents EPDs. EPDs can be utilized to measure e-beam parameters by changing the frequency in the TWT-system. For a practical scenario, if we have an e-beam with an unknown u_0 in the predetermined range, we can vary the operating frequency to observe EPD and find the corresponding u_0 .

The eigenvalues at EPDs are extremely sensitive to perturbations of parameters of the system [45]. Here we establish that a system's sensitivity to a specific parameter variation is boosted by the eigenmodes' degeneracy. For instance, let us consider the EPD in Fig. 4 at $f_e = 16.82$ GHz. In order to measure the sensitivity of the wavenumber to frequency variation, the system's relative perturbation parameter is defined as $\Delta = (f - f_e)/f_e$. Consequently, the perturbed

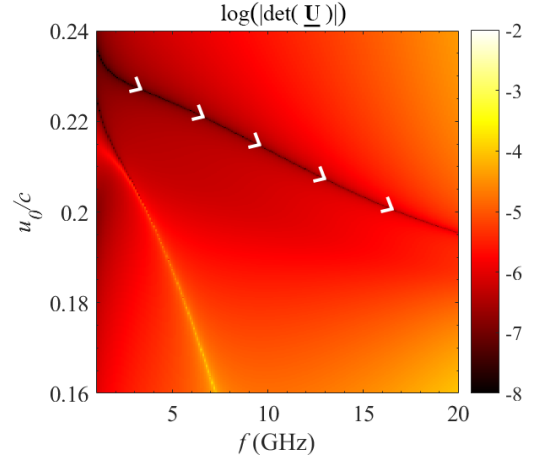


Fig. 6. Determinant of the similarity transformation matrix $\underline{\mathbf{U}}$ varying f and u_0 . The black curve under the white arrows denotes the location of the exceptional degeneracy.

system matrix $\underline{\mathbf{M}}(\Delta)$ has two degenerate eigenvalues (i.e., the wavenumbers) occurring at the EPD shift considerably due to a small perturbation in frequency, resulting in two separate eigenvalues $k_n(\Delta)$, with $n = 1, 2$, close to the EPD. These two perturbed eigenvalues are estimated by using a convergent Puiseux series, where the coefficients are calculated using the explicit formulas given in [46]. The approximation of $k_n(\Delta)$ around a second-order EPD is given by

$$k_n(\Delta) \approx k_e + (-1)^n \alpha_1 \sqrt{\Delta} + \alpha_2 \Delta. \quad (16)$$

Following [46], α_1 and α_2 are calculated by

$$\alpha_1 = \sqrt{\left(-\frac{\partial H}{\partial \Delta}(\Delta, k) \right)}, \quad (17)$$

$$\alpha_2 = -\frac{-(\alpha_1^3 \frac{1}{3!} \frac{\partial^3 H}{\partial k^3}(\Delta, k) + \alpha_1 \frac{\partial^2 H}{\partial k \partial \Delta}(\Delta, k))}{2\alpha_1 (\frac{1}{2!} \frac{\partial^2 H}{\partial k^2}(\Delta, k))}, \quad (18)$$

evaluated at the EPD, i.e., at $\Delta = 0$ and $k = k_e$, where $H(\Delta, k) = \det[\underline{\mathbf{M}}(\Delta) - k\underline{\mathbf{I}}]$. Eq. (16) indicates that for a small perturbation $|\Delta| \ll 1$ in frequency, the eigenvalues change dramatically from their original degenerate value due to the square root dependence. The results in Figs. 7(a) and (b) produce the two branches of the exact perturbed eigenvalues k_n obtained from the eigenvalue problem when the perturbation Δ is applied. These figures explain that such perturbed eigenvalues could be estimated with high accuracy by using the Puiseux series truncated to its second order. Next, we analyze the sensitivity to variations in u_0 by defining $\Delta = (u_0 - u_{0,e})/u_{0,e}$ and apply the same procedure to achieve a Puiseux series coefficients. The calculated results for perturbation in u_0 are illustrated in Figs. 7(c) and (d), which demonstrate the bifurcation and high-sensitivity of the wavenumbers to perturbation near the EPD.

In conclusion, we have investigated the occurrence of EPDs in a system consisting of a linear e-beam interacting with a guided EM wave. We have focused on a practical example

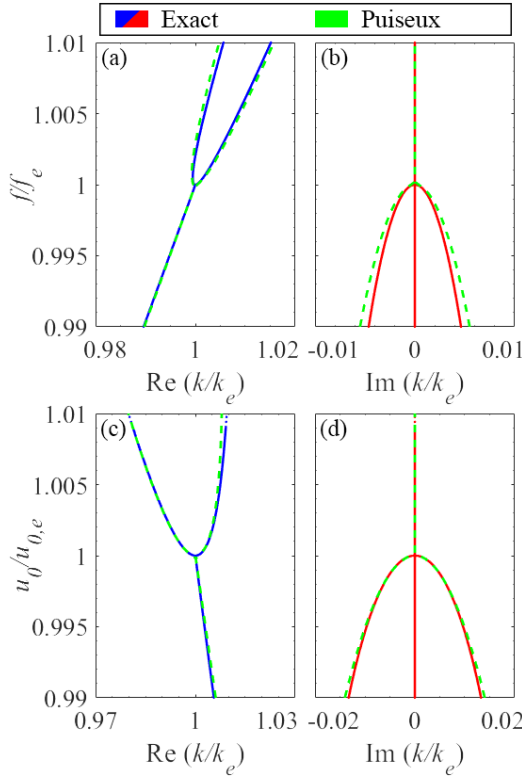


Fig. 7. The Puiseux fractional power expansion up to the second-order approximates the dispersion diagram variation by frequency and u_0 , further demonstrating that the bifurcation point is the EPD. (a) and (b) Complex-valued wavenumbers when frequency is changed, and the required coefficients are calculated as $\alpha_1 = 99.48 \text{ m}^{-1}$ and $\alpha_2 = 1854.45 \text{ m}^{-1}$. (c) and (d) Complex-valued wavenumbers when u_0 is changed, and the required coefficients are calculated as $\alpha_1 = 175.59 \text{ m}^{-1}$ and $\alpha_2 = -764.07 \text{ m}^{-1}$.

where the EM wave is guided by a helix-based SWS, but the same model can be applied to other guiding geometries. We have considered realistic parameters for the e-beam's space-charge effect and waveguide's dispersion of phase velocity and Pierce (interaction) impedance in the developed model. We have discovered the necessary and required conditions to establish an EPD in TWT-system. Then, we have discussed how the wavenumbers of the modes participating in an EPD are extremely sensitive to system perturbations. We have shown how a bifurcation point well describes such perturbation near an EPD, also demonstrated by employing the Puiseux fractional power series expansion. The very high sensitivity to variations can pave the way to new accurate measurement techniques of e-beam parameters.

ACKNOWLEDGMENTS

This material is based upon work supported by the Air Force Office of Scientific Research award number FA9550-18-1-0355, award number FA9550-19-1-0103, and award number FA9550-20-1-0409. The authors are thankful to DS SIMULIA for providing CST Studio Suite that was instrumental in this study.

APPENDIX

A. Electron Beam Model

There are various approaches to analyzing an electron beam's (e-beam) interaction with a traveling electromagnetic (EM) wave on a circuit. The classical small-signal theory by J. R. Pierce is one of the approaches that still use these days for the modeling and designing of traveling wave tubes (TWT). Pierce's model includes a qualitative description of traveling wave interaction that is explained in [26], [27]. Many of the parameters defined by Pierce are now part of the accepted vocabulary in traveling wave tube research and industry. For these reasons, and because the Pierce theory provides considerable physical insight into TWT mechanics, the basic elements of the Pierce theory will be described here, together with generalizations that have been adopted.

In this section, we show the fundamental equations that describe the e-beam dynamics in both space and time. We follow the linearized equations that describe the space-charge wave as originally presented by Pierce [27]. We assume the e-beam is made of a narrow cylindrical pencil beam of electrons, which is subject to an axial (i.e., longitudinal) electric field, assumed constant over the beam's transverse cross-section; we also consider purely longitudinal electron motion due to a strong externally applied axial magnetic field which confines the beam. Because of this, the beam is described by a one-dimensional function, as will be shown. The beam's total linear charge density $\rho_b^{tot}(z, t)$, and electron velocity $u_b^{tot}(z, t)$ are represented as

$$\rho_b^{tot}(z, t) = \rho_0 + \rho_b(z, t), \quad (19)$$

$$u_b^{tot}(z, t) = u_0 + u_b(z, t), \quad (20)$$

where the subscripts "0" and "b" denote the d.c. (average value) and the a.c. (alternate current, i.e., modulation), respectively. In the above equations, ρ_0 is negative and $u_b^{tot}(z, t)$ is the electron speed in the z -direction. The basic equation that is governing the charges' longitudinal motion is

$$\frac{du_b^{tot}(z, t)}{dt} = -\eta e_z, \quad (21)$$

where $\eta = e/m = 1.758829 \times 10^{11} \text{ C/kg}$ is the charge to mass ratio of an electron, the electron charge is equal to $-e$, and m is the rest mass of the electron. The term e_z is the total a.c. electric field in the z -direction, provided by the superposition of two fields as $e_z = e_w + e_p$, where e_w is the z -polarization of the electric field pertaining to the EM mode guided in the waveguide, and e_p is the electric field generated by space-charge, as is discussed later in this section. Following [27], we rewrite the total derivative on the left-hand side of Eq. (21) as

$$\frac{d(u_0 + u_b)}{dt} = \frac{\partial u_b}{\partial t} + (u_0 + u_b) \frac{\partial u_b}{\partial z} + \frac{\partial u_0}{\partial t} + (u_0 + u_b) \frac{\partial u_0}{\partial z}. \quad (22)$$

Some terms on this equation vanish because $\partial u_0/\partial t = 0$, and $\partial u_0/\partial z = 0$. Using a small-signal approximation, we assume that the modulating velocity u_b is small with respect to u_0 ; hence the term $u_b \partial u_b/\partial z$, which is a product of two a.c. small quantities, is negligible with respect to the two other terms involving u_b . Therefore, in our small-signal theory, we neglect the term $u_b \partial u_b/\partial z$, as was originally done by Pierce [27]. Thus, Eq. (21) is rewritten as

$$\frac{\partial u_b(z, t)}{\partial t} + u_0 \frac{\partial u_b(z, t)}{\partial z} = -\eta e_z. \quad (23)$$

For convenience, we define the equivalent kinetic beam current as

$$\begin{aligned} i_b^{tot}(z, t) &= u_b^{tot}(z, t) \rho_b^{tot}(z, t) = u_0 \rho_0 + u_0 \rho_b + u_b \rho_0 + u_b \rho_b \\ &\approx -I_0 + i_b(z, t), \end{aligned} \quad (24)$$

Note that we assume a small-signal modulation in the beam speed and charge density, i.e., we consider a linear model by neglecting the term $u_b \rho_b$ in Eq. (24). Here, the term $u_b \rho_b$ is a product of two small a.c. quantities and is neglected. The a.c. and d.c. portions of the e-beam current are

$$\begin{cases} i_b(z, t) = u_0 \rho_b + u_b \rho_0 \\ -I_0 = u_0 \rho_0 \end{cases} \quad (25)$$

Moreover, we consider the continuity equation or conservation of charge,

$$\frac{\partial i_b^{tot}(z, t)}{\partial z} = -\frac{\partial \rho_b^{tot}(z, t)}{\partial t}, \quad (26)$$

which is rewritten as follows

$$\frac{\partial i_b(z, t)}{\partial z} - \frac{\partial I_0}{\partial z} = -\frac{\partial \rho_b(z, t)}{\partial t} - \frac{\partial \rho_0}{\partial t}. \quad (27)$$

We know that I_0 and ρ_0 are d.c. quantities, i.e., their derivatives are vanishing, so the continuity equation leads finally to

$$\frac{\partial i_b(z, t)}{\partial z} = -\frac{\partial \rho_b(z, t)}{\partial t}. \quad (28)$$

For a non-relativistic beam, it is convenient to define an equivalent kinetic beam voltage as

$$v_b^{tot}(z, t) = \frac{(u_b^{tot}(z, t))^2}{2\eta} = \frac{u_0^2 + u_b^2 + 2u_0 u_b}{2\eta} \approx V_0 + v_b(z, t), \quad (29)$$

and as explained earlier, based on the small-signal approximation, we neglect the nonlinear term u_b^2 , and separate the a.c. and d.c. terms as

$$\begin{cases} v_b(z, t) = \frac{u_0 u_b}{\eta} \\ V_0 = \frac{u_0^2}{2\eta} \end{cases} \quad (30)$$

By combining Eqs. (28), (25), and (30) we find

$$\frac{\partial i_b(z, t)}{\partial z} = \frac{\eta \rho_0}{u_0^2} \frac{\partial v_b(z, t)}{\partial t} - \frac{1}{u_0} \frac{\partial i_b(z, t)}{\partial t}. \quad (31)$$

Moreover, by using Eqs. (23), and (30) we write

$$\frac{\partial v_b(z, t)}{\partial z} + \frac{1}{u_0} \frac{\partial v_b(z, t)}{\partial t} = -e_z. \quad (32)$$

Eqs. (31) and (32) are the two equations governing the e-beam's dynamic based on the model adopted. In the next step, we elaborate more on the bunching and debunching effects of the convection beam current in a traveling-wave field. As was stated previously, the total longitudinal field e_z is represented as the sum of the electric field of the EM mode in the slow-wave structure (SWS) and the a.c. space-charge field, $e_z = e_w + e_p$, where e_w is the z -component of the purely vortical field $\mathbf{e}_w = \text{curl} \mathbf{b}_w$, where \mathbf{b}_w is a magnetic field of the EM mode in the passive SWS; therefore, $\text{div} \mathbf{e}_w = 0$ [31], [47]. The waveguide EM field e_w is provided by [27]

$$e_w = -a \frac{\partial v}{\partial z}, \quad (33)$$

where v is the voltage in the equivalent transmission line (TL) which describes how EM fields propagate in the waveguide, as will be explained further in the next section. In order to model the interaction strength between the e-beam and TL, we have generalized the coupling strength using the coefficient a that represents the strength of interaction between the e-beam and the guided EM mode, as was also described in [34], [33], [32]. Physically, this coupling strength coefficient describes how strongly the electric field of a mode in the SWS affects electron motion.

The space-charge field e_p is longitudinal, i.e., polarized along the z -direction, and it is generated by electron bunching. It is determined from the Poisson equation $\nabla \cdot \mathbf{e}_p = \rho_v/\epsilon_0$. The volumetric charge density ρ_v is assumed to be only z -dependent, and it is related to the linear charge density by $\rho_b = \rho_v A$, where A is the transverse cross-sectional area of the beam. This leads to

$$\frac{\partial e_p}{\partial z} = \frac{\rho_b}{A \epsilon_0}. \quad (34)$$

Differentiating in time on both sides of Eq. (34) and using Eq. (28), the above equation is reduced to

$$\frac{\partial^2 e_p}{\partial t \partial z} = -\frac{1}{A \epsilon_0} \frac{\partial i_b}{\partial z}. \quad (35)$$

Now, we rewrite all the equations that will be used to find the hybrid eigenmodes in the phasor domain assuming implicitly the $\exp(j\omega t)$ time dependence for monochromatic fields. Eq. (31) is rewritten in terms of the beam's equivalent voltage and current phasors as

$$\frac{\partial I_b}{\partial z} = -j \frac{\omega I_0}{2V_0 u_0} V_b - j \frac{\omega}{u_0} I_b, \quad (36)$$

which represents the first of the two main equations that govern the beam dynamics. The second equation is obtained from Eq. (32) based on the following steps. In the phasor domain, $E_z = E_w + E_p$, and Eq. (33) is written as $E_w(\omega) = -a (dV/dz)$. Then, considering the well-known telegrapher's equation in the phasor domain $dV/dz = -ZI$, where Z is the series per-unit-length TL distributed impedance, and I is the

current in the equivalent TL (see next section), the longitudinal EM-guided field is found as

$$E_w(\omega) = aZI. \quad (37)$$

By using the phasor form, Eq. (35) integrated in the z -domain is rewritten as

$$E_p(z) = j \frac{1}{A\varepsilon_0\omega} I_b(z) + \text{const.} \quad (38)$$

Finally, using the obtained expression for total longitudinal field $E_z = E_w + E_p$, Eq. (32) in the phasor domain yields

$$\frac{\partial V_b}{\partial z} = -aZI - j \frac{\omega}{u_0} V_b - j \frac{1}{A\varepsilon_0\omega} I_b, \quad (39)$$

which connects the EM mode equivalent current to the e-beam kinetic voltage and current. This is the second main equation that governs the beam's dynamics.

So far, we have achieved *two* important first-order linear differential equations that describe the dynamics of the e-beam kinetic voltage and current, Eq. (39) and Eq. (36), respectively. As we observe in Eq. (36), the e-beam current is only associated with e-beam parameters, whereas Eq. (39) indicates that TL parameters (in this case, Z and I) are also required to calculate e-beam voltage. In Eq. (39), space-charge fields describe repulsive forces in dense beams of charged particles. These forces induce oscillations of particles at a plasma frequency, which, in a moving medium, have the form of a propagating wave (i.e., the space-charge wave). The plasma frequency is given by

$$\omega_p = \sqrt{-\frac{\rho_0\eta}{A\varepsilon_0}} = \sqrt{\frac{I_0 u_0}{2V_0 A\varepsilon_0}}. \quad (40)$$

In reality, the beam is enclosed in a metallic structure that affects the propagation of space-charge waves. Thus, the plasma frequency of the e-beam, ω_p , is effectively decreased, as compared to its value in the case of an infinite transverse cross section, to a reduced plasma frequency ω_q [48]. Therefore, it is important to calculate the reduced plasma frequency ω_q . This is done by accounting for the reduction factor associated to the plasma frequency $R_{sc} = \omega_q/\omega_p$ that accounts for the metallic tunnel. In the specific case of a thin tape helix TWT (HTWT) with a pencil e-beam, Branch and Mihran found that the helix can be approximated with a perfectly conducting metallic cylinder of the same internal radius [48]. In this paper we have used a plasma frequency reduction factor equal to $R_{sc} = 0.12$, which was calculated for the designed SWS using the software LATTE [42], [29], [43]. To better estimate a TWT performance, one simply replaces ω_p with ω_q in the fundamental equations. Therefore, we rewrite Eq. (39) as

$$\frac{dV_b}{dz} = -aZI - j \frac{\omega}{u_0} V_b - j \frac{2V_0\omega_q^2}{\omega I_0 u_0} I_b. \quad (41)$$

The first term on the right-hand side in Eq. (41) shows the role of the electric field of the waveguide EM mode in the e-beam equations.

B. Electromagnetic Field in the Waveguide Represented by an Equivalent Transmission Line and Interaction with the Beam's Charge Wave

In the TWT-system, the flowing electrons interact with a surrounding circuit. The convection current in the beam causes current to be induced in the circuit. This induced current adds to the current already presented in the circuit, causing the circuit power to increase with distance as power is extracted from the e-beam. We model the SWS using an equivalent TL whose equations are

$$\frac{dV}{dz} = -ZI, \quad (42)$$

$$\frac{dI}{dz} = -YV + i_s. \quad (43)$$

Here, V indicates the equivalent voltage (related to the electric field), and I indicates the equivalent current (related to the magnetic field) in the phasor domain, as explained in [35], [49]. Furthermore, Z is the distributed series impedance per-unit-length, and Y is the distributed shunt admittance per-unit-length. In the above equation, the term i_s represents a distributed current generator [27], [33] that accounts for the effect of the electron stream flowing in the SWS on the EM field whose expression is given by $i_s = -a(dI_b/dz)$. We substitute dI_b/dz in this latter equation with Eq. (36). Then, we obtain the set of two fundamental equations for the equivalent TL

$$\frac{dV}{dz} = -ZI, \quad (44)$$

$$\frac{dI}{dz} = -YV + ja \frac{\omega I_0}{2V_0 u_0} V_b + ja \frac{\omega}{u_0} I_b. \quad (45)$$

In the case of a lossless and non-dispersive waveguide, one has $Z = j\omega L$ and $Y = j\omega C$; however, it is important to note that these equations are here generalized for realistic lossy and dispersive waveguides by accounting for the more complex frequency dependence in $Z(\omega)$ and $Y(\omega)$. Indeed, in realistic systems like the one discussed in this paper, the dispersive waveguide is described by parameters $Z(\omega)$ and $Y(\omega)$ with nonlinear frequency dependence. This more involved frequency dispersion can be equivalently accounted for by defining a dispersive inductance and capacitance per-unit-length as $Z = j\omega L(\omega)$ and $Y = j\omega C(\omega)$ [29], [30], [41].

As a final step, we now summarize the system of four equations comprising the differential equations in Eqs. (36), (41), (44), and (45). This system describes the full dynamics of the linearized (small-signal) model in terms of the equivalent TL voltage and current, $I(z)$ and $V(z)$, as well as the charge-wave current and kinetic voltage, $I_b(z)$ and $V_b(z)$, respectively. We conveniently define a space-varying state vector composed of these four EM-field and charge-wave variables as

$$\Psi(z) = \begin{bmatrix} V(z) \\ I(z) \\ V_b(z) \\ I_b(z) \end{bmatrix}. \quad (46)$$

Without loss of generality, we assume that the TL is homogeneous (i.e., z -invariant), as was originally done by Pierce [27], and we write the four fundamental equations in matrix form as

$$\partial_z \Psi(z) = -j \underline{\mathbf{M}} \Psi(z), \quad (47)$$

where $\underline{\mathbf{M}}$ is a 4×4 system matrix [24]

$$\underline{\mathbf{M}} = \begin{bmatrix} 0 & -jZ & 0 & 0 \\ -jY & 0 & -ag & -a\beta_0 \\ 0 & -jaZ & \beta_0 & R_p \\ 0 & 0 & g & \beta_0 \end{bmatrix}. \quad (48)$$

In the above matrix, we have defined the set of parameters as

$$\beta_0 = \frac{\omega}{u_0}, \quad (49)$$

$$g = \frac{1}{2} \frac{I_0 \beta_0}{V_0}, \quad (50)$$

$$R_p = \frac{1}{A \varepsilon_0 \omega} = \frac{2V_0 \omega_q^2}{\omega I_0 u_0}, \quad (51)$$

where β_0 is beam equivalent propagation constant, and g is a parameter related to the e-beam [24]. In this formulation, we have considered the effect of the bunching of the convection beam current in a traveling wave field using the R_p term in the above matrix, as was done in [36], [37]. This description in terms of a multidimensional first-order differential equation in Eq. (47) is ideal for exploring the occurrence of an exceptional point of degeneracy (EPD) in the system since an EPD is a degeneracy associated with two or more coalescing eigenmodes. In other words, EPDs occur when the system matrix $\underline{\mathbf{M}}$ is similar to a matrix that contains a nontrivial Jordan block. In general, there are four independent eigenmodes and each eigenmode is described by an eigenvector Ψ .

C. Dispersion Equation

To obtain the dispersion equation or characteristic equation, we search for the solution of the form $\Psi(z) = \Psi e^{-jkz}$, where k is the complex-valued wavenumber of the hybrid mode (hybrid because a mode is made of both EM and charge wave components). The four wavenumbers are obtained by solving

$$\det(\underline{\mathbf{M}} - k \underline{\mathbf{I}}) = \det \begin{bmatrix} -k & -jZ & 0 & 0 \\ -jY & -k & -ag & -a\beta_0 \\ 0 & -jaZ & -k + \beta_0 & R_p \\ 0 & 0 & g & -k + \beta_0 \end{bmatrix} = 0. \quad (52)$$

After some mathematical calculations, the dispersion equation is expressed as

$$D(\omega, k) = k^4 - k^3(2\beta_0) + k^2(\beta_0^2 - gR_p + ZY - ja^2Zg) - k(2ZY\beta_0) + ZY(\beta_0^2 - gR_p) = 0. \quad (53)$$

Furthermore, the dispersion equation can be rewritten in the convenient form

$$(k^2 + ZY) ((k - \beta_0)^2 - R_p g) = ja^2 g Z k^2, \quad (54)$$

or we can rewrite it as [33]

$$(k - \beta_0)^2 - \frac{ja^2 g Z k^2}{k^2 + ZY} = g R_p. \quad (55)$$

The cold circuit phase propagation constant is $\beta_c = \sqrt{-ZY}$, and we also used the definition $\beta_q = \omega_q / u_0 = \sqrt{R_p g}$ which represents the phase constant of the space charge wave traveling with a phase velocity equal to the average electron velocity and at an angular frequency equal to ω_q . So, the dispersion characteristic equation is equivalently rewritten as

$$(k^2 - \beta_c^2) ((k - \beta_0)^2 - \beta_q^2) = ja^2 g Z k^2. \quad (56)$$

The right-hand side describes the coupling strength between the two guiding systems: the wavenumber dispersion in the isolated EM waveguide (i.e., without e-beam interaction) would be described by $(k^2 - \beta_c^2) = 0$, and the wavenumber dispersion in the isolated charge wave (i.e., without interacting with the guided EM wave) would be described by $((k - \beta_0)^2 - \beta_q^2) = 0$. It is convenient to define the circuit characteristic impedance and e-beam impedance as

$$Z_c = \frac{Z}{j\beta_c} = \sqrt{\frac{Z}{Y}}, \quad (57)$$

$$Z_0 = \frac{V_0}{I_0}. \quad (58)$$

Pierce defined the dimensionless gain parameter C_P , and called it ‘‘gain parameter’’ [28],

$$C_P^3 = \frac{Z_c}{4Z_0}. \quad (59)$$

Pierce’s gain parameter, C_P , is a measure of the intensity of the interaction between the e-beam and SWS. The characteristic impedance of the equivalent TL Z_c , is also called the interaction impedance or Pierce impedance since it affects the value of Pierce’s gain parameter. Consequently, the above dispersion equation is rewritten in terms of Pierce’s gain parameter as

$$(k^2 - \beta_c^2) ((k - \beta_0)^2 - \beta_q^2) = -2a^2 C_P^3 \beta_c \beta_0 k^2. \quad (60)$$

It may be convenient to consider a modified Pierce gain parameter to account for more realistic EM-beam coupling factors due to the extra coupling strength coefficient we explicitly consider in this paper, as

$$C_{P,m}^3 = a^2 C_P^3. \quad (61)$$

By using this new modified Pierce gain parameter, the dispersion equation expressed in Eq. (60) reduces to

$$(k^2 - \beta_c^2) ((k - \beta_0)^2 - \beta_q^2) = -2C_{P,m}^3 \beta_c \beta_0 k^2. \quad (62)$$

Note that the term $C_{P,m}^3$ on the right side determines the coupling strength between the two dispersion equations of the isolated waveguide and charge-wave guiding systems. If the wavenumber of the hybrid mode, k , in the above equation is solved versus angular frequency, ω , it is worth recalling that the wavenumber of the EM wave in the cold SWS, β_c , also depends on frequency if we consider the waveguide dispersion in our calculations. Furthermore, the Pierce gain parameter $C_{P,m}^3$ also depends on frequency when the cold SWS dispersion makes the characteristic impedance frequency-dependent, aside from the obvious frequency-dependence of β_0 . Furthermore, R_{sc} may also exhibit a slight frequency variation, though it is assumed constant in this paper based on its numerical estimation as described in Appendix A.

An alternative description of the hybrid modes is provided in terms of their phase velocities $v = \omega/k$, rather than their wavenumbers, as was done in [32]. Accordingly, the dispersion equation takes the form of

$$\frac{(v - u_0)^2}{v^2} + \frac{ja^2 Z g u_0^2}{v^2 \beta_c^2 - \omega^2} = \frac{\omega_q^2}{\omega^2}. \quad (63)$$

D. EPD Condition

The solutions of our dispersion equations lead to four modal complex-valued wavenumbers that represent the four hybrid modes in the system. A second-order EPD occurs when two of these eigenmodes coalesce in their eigenvalues and eigenvectors, which means that the matrix $\underline{\mathbf{M}}$ is similar to a matrix that contains a Jordan block of order two [17], [24]. In this case, a necessary condition to have second-order EPD is to have two repeated eigenvalues, which means that the dispersion equation should have two repeated roots as

$$D(\omega_e, k) \propto (k - k_e)^2, \quad (64)$$

where ω_e and k_e are the degenerate angular frequency and wavenumber in EPD condition, respectively. The relation in Eq. (64), which guarantees to have two coalescing wavenumbers, is satisfied when

$$D(\omega_e, k_e) = 0, \quad (65)$$

$$\left. \frac{\partial D(\omega_e, k)}{\partial k} \right|_{k=k_e} = 0. \quad (66)$$

These two conditions are rewritten, respectively, in the below forms

$$\begin{aligned} k_e^4 - k_e^3(2\beta_0) + k_e^2(\beta_0^2 - gR_p + Z_e Y_e - ja^2 Z_e g) \\ - k_e(2Z_e Y_e \beta_0) + Z_e Y_e (\beta_0^2 - gR_p) = 0, \end{aligned} \quad (67)$$

$$\begin{aligned} 4k_e^3 - 3k_e^2(2\beta_0) + 2k_e(\beta_0^2 - gR_p + Z_e Y_e - ja^2 Z_e g) \\ - (2Z_e Y_e \beta_0) = 0. \end{aligned} \quad (68)$$

In the above equations, subscript "e" in different parameters indicates the value at the EPD. The TL distributed series impedance Z_e , and shunt admittance Y_e that provide the EPD are determined after making some mathematical manipulations

in the two above conditions. First, we use Eq. (67) to get Y_e in terms of Z_e and other system parameters as

$$Y_e = \frac{-k_e^4 + k_e^3(2\beta_0) - k_e^2(\beta_0^2 - gR_p - ja^2 Z_e g)}{Z_e ((k_e - \beta_0)^2 - gR_p)}, \quad (69)$$

then we substitute this relation into Eq. (68) and solve it for Z_e , which is found to be

$$Z_e = \frac{j((k_e - \beta_0)^2 - R_p g)^2}{a^2 g(-\beta_0^2 + k_e \beta_0 + R_p g)}. \quad (70)$$

Finally, we substitute back the impedance value obtained from Eq. (70) in the admittance value calculated in Eq. (69) to find admittance

$$Y_e = \frac{ja^2 g_e k_e^3 (k_e - \beta_0)}{((k_e - \beta_0)^2 - R_p g)^2}. \quad (71)$$

To realize an EPD, the TL series impedance $Z = Z_e$ and shunt admittance $Y = Y_e$ need to satisfy Eqs. (70) and (71). Assuming that the EPD conditions in Eqs. (70) and (71) are satisfied, then the degenerate wavenumber k_e is determined by the product of Eqs. (70) and (71)

$$Z_e Y_e = \frac{-k_e^3 (k_e - \beta_0)}{(-\beta_0^2 + k_e \beta_0 + R_p g)}. \quad (72)$$

We know that $\beta_{c,e}^2 = -Z_e Y_e$ and $\beta_q^2 = R_p g$, so we calculate k_e by solving the equation

$$\beta_{c,e}^2 \beta_q^2 = (k_e^3 - \beta_{c,e}^2 \beta_0)(k_e - \beta_0). \quad (73)$$

Since we search for solution of the form $\Psi(z) = \Psi_n e^{-jk_n z}$, the eigenvectors Ψ_n of the system are determined by solving the eigenvalue problem $\underline{\mathbf{M}}\Psi_n = k_n \Psi_n$, or we can write it as below

$$(\underline{\mathbf{M}} - k_n \underline{\mathbf{I}})\Psi_n = 0, \quad (74)$$

where k_n with $n = 1, 2, 3, 4$ are the wavenumbers, and they are determined from Eq. (74). By solving Eq. (74), the eigenvectors are written in the form of

$$\Psi_n = \begin{bmatrix} (k_n - \beta_0)^2 - R_p g \\ j \frac{k_n}{Z} ((k_n - \beta_0)^2 - R_p g) \\ ak_n (k_n - \beta_0) \\ agk_n \end{bmatrix}. \quad (75)$$

At the second-order EPD investigated in this paper, two of these four eigenvectors coalesce.

E. Theoretical Gain Calculation

As we discuss in the main body of the paper, the frequency-dependent parameters describing EM propagation in the dispersive and lossy waveguide in the proposed model have a vital role in the accuracy of the calculated results. In order to test the accuracy of the proposed model, we need to compare the theoretically calculated results with those numerically obtained from commercial software. The software LATTE is used to calculate the gain versus frequency of the helix

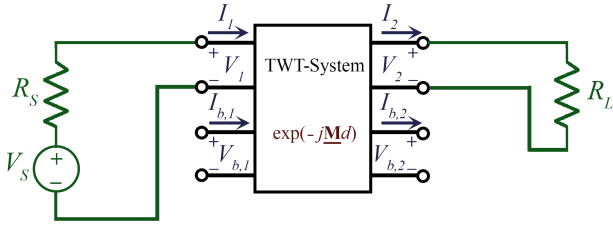


Fig. 8. Circuit model that we use for gain calculation.

TWT amplifier. We use our theoretical method to calculate the power gain versus input signal frequency. The utilized circuit model is illustrated in Fig. 8. The TWT-system is modeled by the system matrix $\underline{\mathbf{M}}$, and we use the input state vector of $\Psi_1 = [V_1, I_1, V_{b,1}, I_{b,1}]^T$, calculated at $z = 0$, and an output state vector $\Psi_2 = [V_2, I_2, V_{b,2}, I_{b,2}]^T$ is calculated at $z = d$, i.e., at the end of the SWS. Here $d = Nl$ is the SWS length, where N indicates the number of unit-cells and l is the SWS period in the z -direction. The output state vector is calculated as

$$\Psi_2 = \exp(-j\mathbf{M}d)\Psi_1, \quad (76)$$

We considered a helix SWS made of $N = 160$ turns, and simulated results are based on this assumption. In our model, we use the boundary condition at $z = 0$ and $z = d$ provided by the equations

$$\begin{cases} V_{b1} = 0 \\ I_{b1} = 0 \\ V_1 + I_1 R_S = V_S \\ V_2 - I_2 R_L = 0 \end{cases} \quad (77)$$

In these equations, the terminations R_S (generator resistance) and R_L (load) are assumed to be equal to the frequency-dependent characteristic impedance of SWS Z_c (vary with frequency, to simulate matching), and V_S is the voltage source. Then, we solve these equations at each frequency and calculate the effective current and voltage at the output of the TL (I_2 , V_2). We calculate the output power $P_{out} = |V_2|^2 / (2R_L)$, and the available input power $P_{avail} = |V_S|^2 / (8R_S)$, to obtain the frequency-dependent gain $G = P_{out} / P_{avail}$, for the TWT-system. As explained above and in the main body of the paper, we have introduced the coupling strength coefficient a , in our equations, which describes the strength of beam-EM mode interaction in the system. The value of a must be optimized in order to obtain good agreement between the theoretical model and simulation results. The optimized value for the designed helix TWT is calculated as $a = 0.527$. With this coupling strength coefficient, the theoretical and simulated gain results are in agreement over the frequency range shown in the main body of the paper. The agreement between the theoretical and simulated gain demonstrates the effectiveness of the theoretical model.

F. Comparison to Lagrangian Model

The Euler-Lagrange equations associated with the Lagrangian are the following system of second-order differen-

tial equations. Without loss of generality, we rewrote these equations in the case of a single stream e-beam and a single TL [34], [32]. All required parameters for this model are summarized in Tables (I) and (II), and readers can find more details about this model in [32]. The basic equations of Lagrangian model are represented as

$$L\partial_t^2 Q - \partial_z [C^{-1}(\partial_z Q + b\partial_z q)] = 0, \quad (78)$$

$$\frac{1}{\beta}(\partial_t + \dot{v}\partial_z)^2 q + \frac{4\pi}{\sigma_B} q - b\partial_z [C^{-1}(\partial_z Q + b\partial_z q)] = 0. \quad (79)$$

TABLE I
E-BEAM PARAMETERS LIST IN LAGRANGIAN MODEL

Name	Value
e-beam steady velocity	\dot{v}
Number of electron density	\hat{n}
Stream intensity	$\beta = \frac{\sigma_B}{4\pi} R_{sc}^2 \omega_p^2 = \frac{R_{sc}^2 e^2}{m} \hat{N}$
Plasma frequency	$\omega_p^2 = \frac{4\pi \hat{n}_s e^2}{m}$
Plasma frequency reduction factor	R_{sc}
Beam current	i
Number of electron per unit of length	$\hat{N} = \sigma_B \hat{n}$
Coupling between e-beam and MTL	$0 < b < 1$
Beam area	σ_B

TABLE II
TL PARAMETERS LIST IN LAGRANGIAN MODEL

Name	Value
Series inductance per-unit-length	L
Shunt capacitance per-unit-length	C
TL characteristic velocity	$w = \frac{1}{\sqrt{LC}}$
Coupling coefficient	b
TL principal coefficient	$\theta = \frac{b^2}{C}$
TWT principal parameter	$\gamma = \theta\beta = \frac{b^2}{C} \frac{\sigma_B}{4\pi} R_{sc}^2 \omega_p^2$

In the above equations, $Q(z)$ represents the phasor of the total amount of a.c. charge flowing through a section at a given z in the TL, and L and C are the values of inductance and capacitance associated with the single TL. Also, $q(z)$ represents the amount of a.c. stream charges modulating the e-beam, at a given section z , in the second-order differential equations. In this section, we wish to put the equations in the matrix form to solve them. We define the state vector based on charges in the TL and charges in the e-beam as

$$\Psi_Q(z) = \begin{bmatrix} Q(z) \\ \partial_z Q(z) \\ q(z) \\ \partial_z q(z) \end{bmatrix}. \quad (80)$$

Next, we write the Eqs. (78) and (79) in the matrix form

$$\partial_z \Psi_Q(z) = -j \underline{\mathbf{M}}_{QL} \Psi_Q(z), \quad (81)$$

where $\underline{\mathbf{M}}_{QL}$ is a 4×4 system matrix associated to the Lagrangian formulation and the charges-based state vector Ψ_Q , and reads as

$$\underline{\mathbf{M}}_{QL} = \begin{bmatrix} 0 & j & 0 & 0 \\ j(\frac{\beta b^2}{v^2 C} - 1)\omega^2 LC & 0 & -j\frac{b}{v^2}(\omega^2 - \frac{4\pi}{\sigma_B}\beta) & -\frac{2\omega}{v}b \\ 0 & 0 & 0 & j \\ -j\frac{\beta b}{v^2}\omega^2 L & 0 & j\frac{1}{v^2}(\omega^2 - \frac{4\pi}{\sigma_B}\beta) & \frac{2\omega}{v} \end{bmatrix}. \quad (82)$$

By defining $Z = j\omega L$ and $Y = j\omega C$, we rewrite Eq. (82) as

$$\underline{\mathbf{M}}_{QL} = \begin{bmatrix} 0 & j & 0 & 0 \\ j(1 - j\omega\frac{\beta b^2}{v^2 Y})ZY & 0 & -j\frac{b}{v^2}(\omega^2 - \frac{4\pi}{\sigma_B}\beta) & -\frac{2\omega}{v}b \\ 0 & 0 & 0 & j \\ -\omega\frac{\beta b}{v^2}Z & 0 & j\frac{1}{v^2}(\omega^2 - \frac{4\pi}{\sigma_B}\beta) & \frac{2\omega}{v} \end{bmatrix}. \quad (83)$$

Assuming that our solutions have a z -dependence $\Psi(z) = \Psi_Q e^{-jkz}$, the eigenvalue problem reads as,

$$(\underline{\mathbf{M}}_{QL} - k\underline{\mathbf{I}})\Psi_Q = 0. \quad (84)$$

Based on Eq. (83), the eigenvalue problem is reduced to

$$\begin{bmatrix} -k & j & 0 & 0 \\ j(1 - j\omega\frac{\beta b^2}{v^2 Y})ZY & -k & -j\frac{b}{v^2}(\omega^2 - \frac{4\pi}{\sigma_B}\beta) & -\frac{2\omega}{v}b \\ 0 & 0 & -k & j \\ -\omega\frac{\beta b}{v^2}Z & 0 & j\frac{1}{v^2}(\omega^2 - \frac{4\pi}{\sigma_B}\beta) & -k + \frac{2\omega}{v} \end{bmatrix} \Psi_Q = 0. \quad (85)$$

After some simplification, the dispersion equation is expressed as

$$\det(\underline{\mathbf{M}}_{QL} - k\underline{\mathbf{I}}) = k^4 - k^3(\frac{2\omega}{v}) + k^2(\frac{1}{v^2}(\omega^2 - \frac{4\pi}{\sigma_B}\beta) + ZY - j\frac{b^2}{v^2}Z\omega\frac{\beta}{v^2}) - k(ZY\frac{2\omega}{v}) + ZY\frac{1}{v^2}(\omega^2 - \frac{4\pi}{\sigma_B}\beta) = 0. \quad (86)$$

According to the Lagrangian model, the general TWT characteristic equation for the phase velocity $v = \omega/k$ of the hybrid modes turns into

$$v^4 \frac{ZY}{v^2} (\omega^2 - \frac{4\pi}{\sigma_B}\beta) - v^3 (ZY \frac{2\omega^2}{v}) + v^2 \omega^2 (\frac{1}{v^2} (\omega^2 - \frac{4\pi}{\sigma_B}\beta) + ZY - j\frac{b^2}{v^2} Z\omega \frac{\beta}{v^2}) - v (\frac{2\omega^4}{v}) + \omega^4 = 0. \quad (87)$$

After some mathematical manipulation, the characteristic equation is expressed by [32, Chapter 25]

$$\frac{\gamma}{w^2 - v^2} + \frac{(v - \check{v})^2}{v^2} = \frac{1}{\check{\omega}^2}, \quad (88)$$

where $\check{\omega}$ is a dimensionless (normalized) frequency [32, Chapter 25]

$$\check{\omega} = \frac{\omega}{R_{sc}\omega_p}. \quad (89)$$

Finally, for convenience we provide the translation table to transform Lagrangian model parameters used in [32] to the Pierce model parameters used in this paper. The list of transformations is summarized in Table (III).

TABLE III
TRANSLATION FROM LAGRANGIAN MODEL PARAMETERS TO THE PIERCE MODEL PARAMETERS

Lagrangian model	Pierce model
\check{v}	$\frac{\omega}{\beta_0} = u_0$
σ_B	A
β	$\frac{g\omega}{\beta_0^2} = \frac{gu_0}{\beta_0}$
w^2	$-\frac{w^2}{ZY} = \frac{w^2}{\beta_c^2}$
γ	$\frac{a^2}{Y} \frac{jg\omega^2}{\beta_0^2} = \frac{a^2}{Y} jgu_0^2$

In the frequency-dependent SWS model that we have introduced in this paper, we consider two frequency-dependent parameters, i.e., the cold circuit EM phase velocity v_c , and the equivalent TL characteristic impedance Z_c . The same procedure can be used for the demonstrated Lagrangian model in [32]. In the Lagrangian model, the TL principal coefficient, $\theta(\omega)$, and TL characteristic velocity, $w(\omega)$, are the two frequency-dependent parameters in the Lagrangian equations. Equivalently, in the displayed characteristic equation in Eq. (88), the TWT principal parameter, $\gamma(\omega)$, and TL characteristic velocity, $w(\omega)$, are the two frequency-dependent parameters in the Lagrangian model.

G. Space-Charge Effect

Space-charge fields represent repulsive forces in dense beams of charged particles. These forces induce oscillations of particles at a plasma frequency, which, in a moving medium, has the form of a propagating wave (i.e., the space-charge wave). In this paper, we have provided TWT-system equations which account for space-charge effects. This effect can be modeled based on calculations provided in the first section of Appendix for the Lagrangian model of the TWT-system in

[34], [32]. In the first step, we start with the extended equations represented in 47,

$$\begin{cases} \partial_z V = -ZI \\ \partial_z I = -YV + ja \frac{\omega I_0}{2V_0 u_0} V_b + ja \frac{\omega}{u_0} I_b \\ \partial_z V_b = -aZI - j \frac{\omega}{u_0} V_b - j \frac{1}{\omega A \epsilon_0} I_b \\ \partial_z I_b = -j \frac{\omega I_0}{2V_0 u_0} V_b - j \frac{\omega}{u_0} I_b \end{cases} \quad (90)$$

Then, we transform the four first-order differential equations into two second-order differential equations by removing voltages, V and V_b , leading to

$$\begin{cases} \partial_z^2 I - ZYI + a\partial_z^2 I_b = 0 \\ jag\partial_z^2 I - Y\partial_z^2 I_b - j2Y\beta_0\partial_z I_b + Y\beta_0^2 I_b - gYR_p I_b \\ + ja^2 g\partial_z^2 I_b = 0 \end{cases} \quad (91)$$

In the next step, we use the below substitutions for converting currents to charges

$$\begin{cases} I = j\omega Q \\ I_b = j\omega q \end{cases} \quad (92)$$

After some mathematical manipulation, we obtain these equations

$$\begin{cases} L\partial_t^2 Q - \partial_z[C^{-1}(\partial_z Q + a\partial_z q)] = 0 \\ \frac{\beta_0^2}{g\omega}(\partial_t + \frac{\omega}{\beta_0}\partial_z)^2 q + \omega R_p q - a\partial_z[C^{-1}((\partial_z Q + a\partial_z q))] = 0 \end{cases} \quad (93)$$

This set of equations are equivalent to Euler-Lagrange equations, which are presented in Eqs. (78), and (79). The term $\omega R_p q$ is responsible for the space-charge effect. It can also be written as

$$\omega R_p q = \frac{1}{A\epsilon_0} q. \quad (94)$$

On the other hand, in the presented Euler-Lagrange equations, the term $\frac{4\pi}{\sigma_B} q$, accounts for the debunching effect (See Eq. (79)). Since the Gaussian system of units is utilized in the Euler-Lagrange equations, we need to transform parameters to the International System of Units (SI). After performing the mentioned transformation, we obtain the same definition as presented in Eq. 94.

H. An Equivalent Alternative Formulation Based on Charge

As explained in the previous section, we defined matrix equations for the TWT-system as expressed in Eq. (48). In the next step, we start with the substitutions presented in Eq. 92 to convert currents to charges. This leads to modified set of TWT-system equations as

$$\partial_z \begin{bmatrix} V \\ j\omega Q \\ V_b \\ j\omega q \end{bmatrix} = \begin{bmatrix} 0 & -Z & 0 & 0 \\ -Y & 0 & jag & ja\beta_0 \\ 0 & -aZ & -j\beta_0 & -jR_p \\ 0 & 0 & -jg & -j\beta_0 \end{bmatrix} \begin{bmatrix} V \\ j\omega Q \\ V_b \\ j\omega q \end{bmatrix}. \quad (95)$$

The matrix is equivalent to the four equations

$$\begin{cases} \partial_z V = -jZ\omega Q \\ j\omega\partial_z Q = -YV + jagV_b - a\beta_0\omega q \\ \partial_z V_b = -jaZ\omega Q - j\beta_0 V_b + R_p\omega q \\ j\omega\partial_z q = -jgV_b + \beta_0\omega q \end{cases} \quad (96)$$

By combining the equations and performing some mathematical simplification, we remove voltages (V and V_b) from equations and decrease four first-order differential equations into two second-order differential equations based on charge:

$$\begin{cases} \partial_z^2 Q = YZQ - ja^2 gZQ + ja\beta_0\partial_z q - a\beta_0^2 q + agR_p q \\ + ja\beta_0\partial_z q \\ \partial_z^2 q = jagZQ - j\beta_0\partial_z q + \beta_0^2 q - gR_p q - j\beta_0\partial_z q \end{cases} \quad (97)$$

In order to analyze the characteristics of the system like wavenumbers, we rewrite equations in the matrix form. So, we use a state vector based on charge, as was expressed before in Eq. (80), and rewrite Eq. (97) as

$$\partial_z \Psi_Q(z) = -j\mathbf{M}_Q \Psi_Q(z), \quad (98)$$

$$\mathbf{M}_Q = \begin{bmatrix} 0 & j & 0 & 0 \\ jYZ + a^2 gZ & 0 & -ja\beta_0^2 + jagR_p & -2a\beta_0 \\ 0 & 0 & 0 & j \\ -agZ & 0 & j\beta_0^2 - jgR_p & 2\beta_0 \end{bmatrix}. \quad (99)$$

By using the same approach described before, the characteristic equation is calculated from

$$\det(\mathbf{M}_Q - k\mathbf{I}) = \det \begin{bmatrix} -k & j & 0 & 0 \\ jYZ + a^2 gZ & -k & -ja\beta_0^2 + jagR_p & -2s\beta_0 \\ 0 & 0 & -k & j \\ -agZ & 0 & j\beta_0^2 - jgR_p & -k + 2\beta_0 \end{bmatrix} = 0, \quad (100)$$

resulting in the following dispersion equation

$$D(\omega, k) = k^4 - k^3(2\beta_0) + k^2(\beta_0^2 - gR_p + ZY - a^2 jZg) - k(2ZY\beta_0) + ZY(\beta_0^2 - gR_p) = 0. \quad (101)$$

REFERENCES

- [1] D. Shiffler, J. A. Nation, and C. Wharton, "High-power traveling-wave tube amplifier," *Applied physics letters*, vol. 54, no. 7, pp. 674–676, 1989.
- [2] C.-L. Hung, "High-power, stable ka/v dual-band gyrotron traveling-wave tube amplifier," *Applied Physics Letters*, vol. 100, no. 20, p. 203502, 2012.
- [3] C. M. Armstrong, R. Kowalczyk, A. Zubyk, K. Berg, C. Meadows, D. Chan, T. Schoemehl, R. Duggal, N. Hinch, R. B. True *et al.*, "A compact extremely high frequency mpm power amplifier," *IEEE Transactions on Electron Devices*, vol. 65, no. 6, pp. 2183–2188, 2018.

- [4] S. Naqvi, G. Kerslick, J. Nation, and L. Schächter, "Axial extraction of high-power microwaves from relativistic traveling wave amplifiers," *Applied physics letters*, vol. 69, no. 11, pp. 1550–1552, 1996.
- [5] J. X. Qiu, B. Levush, J. Pasour, A. Katz, C. M. Armstrong, D. R. Whaley, J. Tucek, K. Kreischer, and D. Gallagher, "Vacuum tube amplifiers," *IEEE Microwave Magazine*, vol. 10, no. 7, pp. 38–51, 2009.
- [6] W. D. Heiss, "Repulsion of resonance states and exceptional points," *Physical Review E*, vol. 61, no. 1, p. 929, 2000.
- [7] —, "Exceptional points of non-hermitian operators," *Journal of Physics A: Mathematical and General*, vol. 37, no. 6, pp. 2455–2464, Jan 2004.
- [8] A. Figotin and I. Vitebskiy, "Gigantic transmission band-edge resonance in periodic stacks of anisotropic layers," *Physical Review E*, vol. 72, no. 3, p. 036619, Sep 2005.
- [9] M. A. K. Othman and F. Capolino, "Theory of exceptional points of degeneracy in uniform coupled waveguides and balance of gain and loss," *IEEE Transactions on Antennas and Propagation*, vol. 65, no. 10, pp. 5289–5302, Oct 2017.
- [10] K. Rouhi, H. Kazemi, A. Figotin, and F. Capolino, "Exceptional points of degeneracy directly induced by space-time modulation of a single transmission line," *IEEE Antennas and Wireless Propagation Letters*, vol. 19, no. 11, pp. 1906 – 1910, nov 2020.
- [11] A. Figotin and I. Vitebskiy, "Oblique frozen modes in periodic layered media," *Physical Review E*, vol. 68, no. 3, p. 036609, Sep 2003.
- [12] M. A. K. Othman, F. Yazdi, A. Figotin, and F. Capolino, "Giant gain enhancement in photonic crystals with a degenerate band edge," *Physical Review B*, vol. 93, no. 2, p. 024301, Jan 2016.
- [13] H. Kazemi, M. Y. Nada, T. Mealy, A. F. Abdelshafy, and F. Capolino, "Exceptional points of degeneracy induced by linear time-periodic variation," *Physical Review Applied*, vol. 11, no. 1, p. 014007, Jan 2019.
- [14] H. Kazemi, A. Hajiaghajani, M. Y. Nada, M. Dautta, M. Alshetaiwi, P. Tseng, and F. Capolino, "Ultra-sensitive radio frequency biosensor at an exceptional point of degeneracy induced by time modulation," *IEEE Sensors Journal*, vol. 21, no. 6, pp. 7250–7259, Mar 2020.
- [15] C. M. Bender and S. Boettcher, "Real spectra in non-hermitian hamiltonians having PT symmetry," *Physical Review Letters*, vol. 80, no. 24, pp. 2455–2464, Jun 1998.
- [16] J. Schindler, A. Li, M. C. Zheng, F. M. Ellis, and T. Kottos, "Experimental study of active LRC circuits with PT symmetries," *Physical Review A*, vol. 84, no. 4, p. 040101, Oct 2011.
- [17] T. Kato, *Perturbation Theory for Linear Operators*, 2nd ed. Springer-Verlag, Berlin Heidelberg, 1995, vol. 132.
- [18] J. Wiersig, "Sensors operating at exceptional points: General theory," *Physical Review A*, vol. 93, no. 3, p. 033809, Mar 2016.
- [19] P.-Y. Chen, M. Sakhdari, M. Hajizadegan, Q. Cui, M. M.-C. Cheng, R. El-Ganainy, and A. Alu, "Generalized parity-time symmetry condition for enhanced sensor telemetry," *Nature Electronics*, vol. 1, no. 5, pp. 297–304, May 2018.
- [20] H. Hodaie, M.-A. Miri, M. Heinrich, D. N. Christodoulides, and M. Khajavikhan, "Parity-time symmetric microring lasers," *Science*, vol. 346, no. 6212, pp. 975–978, Nov 2014.
- [21] M. A. K. Othman, M. Veysi, A. Figotin, and F. Capolino, "Low starting electron beam current in degenerate band edge oscillators," *IEEE Transactions on Plasma Science*, vol. 44, no. 6, pp. 918–929, Jun 2016.
- [22] M. Veysi, M. A. K. Othman, A. Figotin, and F. Capolino, "Degenerate band edge laser," *Physical Review B*, vol. 97, no. 19, p. 195107, May 2018.
- [23] A. F. Abdelshafy, D. Oshmarin, M. A. Othman, M. M. Green, and F. Capolino, "Distributed degenerate band edge oscillator," *IEEE Transactions on Antennas and Propagation*, 2020.
- [24] T. Mealy, A. F. Abdelshafy, and F. Capolino, "Exceptional point of degeneracy in a backward-wave oscillator with distributed power extraction," *Physical Review Applied*, vol. 14, no. 1, p. 014078, 2020.
- [25] A. Figotin, "Exceptional points of degeneracy in traveling wave tubes," *arXiv preprint arXiv:2012.12849*, 2020.
- [26] J. R. Pierce, "Theory of the beam-type traveling-wave tube," *Proceedings of the IRE*, vol. 35, no. 2, pp. 111–123, 1947.
- [27] —, "Waves in electron streams and circuits," *Bell System Technical Journal*, vol. 30, no. 3, pp. 626–651, 1951.
- [28] —, *Traveling-wave tubes*. D. Van Nostrand Company Inc., 1954.
- [29] J. G. Wohlbiel, J. H. Booske, and I. Dobson, "The multifrequency spectral eulerian (muse) model of a traveling wave tube," *IEEE Transactions on Plasma Science*, vol. 30, no. 3, pp. 1063–1075, 2002.
- [30] M. C. Converse, J. H. Booske, and S. C. Hagness, "Impulse amplification in a traveling-wave tube-i: Simulation and experimental validation," *IEEE transactions on plasma science*, vol. 32, no. 3, pp. 1040–1048, 2004.
- [31] J. W. Gewartowski and H. A. Watson, *Principles of electron tubes: including grid-controlled tubes, microwave tubes, and gas tubes*. Van Nostrand, 1965.
- [32] A. Figotin, *An Analytic Theory of Multi-stream Electron Beams in Traveling Wave Tubes*. World Scientific, 2020.
- [33] V. A. Tamma and F. Capolino, "Extension of the pierce model to multiple transmission lines interacting with an electron beam," *IEEE Transactions on Plasma Science*, vol. 42, no. 4, pp. 899–910, 2014.
- [34] A. Figotin and G. Reyes, "Multi-transmission-line-beam interactive system," *Journal of Mathematical Physics*, vol. 54, no. 11, p. 111901, 2013.
- [35] N. Marcuvitz and J. Schwinger, "On the representation of the electric and magnetic fields produced by currents and discontinuities in wave guides. I," *Journal of Applied Physics*, vol. 22, no. 6, pp. 806–819, 1951.
- [36] M. A. K. Othman, M. Veysi, A. Figotin, and F. Capolino, "Giant amplification in degenerate band edge slow-wave structures interacting with an electron beam," *Physics of Plasmas*, vol. 23, no. 3, p. 033112, Mar 2016.
- [37] M. A. K. Othman, V. A. Tamma, and F. Capolino, "Theory and new amplification regime in periodic multimodal slow wave structures with degeneracy interacting with an electron beam," *IEEE Transactions on Plasma Science*, vol. 44, no. 4, pp. 594–611, Apr 2016.
- [38] J. Hammer, "Coupling between slow waves and convective instabilities in solids," *Applied Physics Letters*, vol. 10, no. 12, pp. 358–360, 1967.
- [39] J. H. Booske and M. C. Converse, "Insights from one-dimensional linearized pierce theory about wideband traveling-wave tubes with high space charge," *IEEE transactions on plasma science*, vol. 32, no. 3, pp. 1066–1072, 2004.
- [40] Y. Han, Y.-W. Liu, Y.-G. Ding, P.-K. Liu, and C.-H. Lu, "Thermal analysis of a helix twt slow-wave structure," *IEEE transactions on electron devices*, vol. 55, no. 5, pp. 1269–1272, 2008.
- [41] A. Setayesh and M. S. Abrishamian, "Pawaic-psaofddt: Particle-wave interaction code with pseudospectral arbitrary-order accurate temporal and spatial derivatives fddt technique for helix twt," *IEEE Transactions on Electron Devices*, vol. 64, no. 11, pp. 4706–4714, 2017.
- [42] T. Antonsen and B. Levush, "Traveling-wave tube devices with nonlinear dielectric elements," *IEEE transactions on plasma science*, vol. 26, no. 3, pp. 774–786, 1998.
- [43] J. Wohlbiel, M. Converse, J. Plouin, A. Rawal, A. Singh, and J. Booske, "Latte/muse numerical suite: An open source teaching and research code for traveling wave tube amplifiers," in *4th IEEE International Conference on Vacuum Electronics, 2003*. IEEE, 2003, pp. 16–17.
- [44] P. Y. Wong, D. Chernin, and Y. Lau, "Modification of pierce's classical theory of traveling-wave tubes," *IEEE Electron Device Letters*, vol. 39, no. 8, pp. 1238–1241, 2018.
- [45] X. Zhou, S. K. Gupta, Z. Huang, Z. Yan, P. Zhan, Z. Chen, M. Lu, and Z. Wang, "Optical lattices with higher-order exceptional points by non-hermitian coupling," *Applied Physics Letters*, vol. 113, no. 10, p. 101108, 2018.
- [46] A. Welters, "On explicit recursive formulas in the spectral perturbation analysis of a Jordan Block," *SIAM Journal on Matrix Analysis and Applications*, vol. 32, no. 1, pp. 1–22, Jan 2011.
- [47] S. E. Tsimring, *Electron beams and microwave vacuum electronics*. NJ: Wiley-Interscience, 2007, vol. 191.
- [48] G. Branch and T. Mihran, "Plasma frequency reduction factors in electron beams," *IRE Transactions on Electron Devices*, vol. 2, no. 2, pp. 3–11, 1955.
- [49] L. B. Felsen and N. Marcuvitz, *Radiation and scattering of waves*. John Wiley & Sons, 1994, vol. 31.